Research Square

Preprints are preliminary reports that have not undergone peer review.
They should not be considered conclusive, used to inform clinical practice,
or referenced by the media as validated information.

Development of MEMS Pressure Sensor with High Proof Pressure for Adjustable Ranges

Mikhail Basov

engineerbasovm@gmail.com

FSUE VNIIA https://orcid.org/0000-0003-0798-4500

Research Article

Keywords: pressure sensor, microassembly design, high proof pressure, low error, residual mechanical stress

Posted Date: February 27th, 2026

DOI: https://doi.org/10.21203/rs.3.rs-8978586/v1

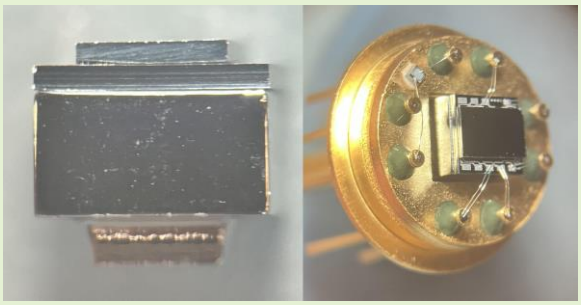
License: This work is licensed under a Creative Commons Attribution 4.0 International License.
Read Full License

Additional Declarations: The authors declare no competing interests.

Development of MEMS Pressure Sensor with High Proof Pressure for Adjustable Ranges up to 10...60 kPa

Mikhail Basov, *PhD, R&D Engineer*

***Abstract* — The various application conditions of MEMS pressure sensors require achieving a wide range of specific parameters. The ability to save pressure sensor by repeated proof pressure is one of the important requirements. The research presents a new microassembly design for the piezoresistive pressure sensor chip for adjustable differential pressure ranges up to 10...60 kPa. The microassembly design contains stops on both sides of the chip to increase the proof pressure to P_{proof} = 1.5 MPa. Additionally, the microassembly also allows for significant improvement of mechanical decoupling of chip from packing and all existing mechanical connections. The research demonstrates the efficiency of using of thermocycling and barocycling for pressure sensor. In results, more than 120 samples of developed pressure sensor have sensitivity S = 0.61 ± 0.15 mV/V/kPa and low error for nonlinearity $2K_{NL}$ < 0.20%/FS, mechanical hysteresis H < 0.10%/FS and mechanical repeatability R < 0.05%/FS, as well as for the effect of overload pressure dU_{Pproof} < 0.30%/FS and all-round compression with pressure of 16 MPa dU_{comp} < 0.15%/FS. The significant advantage of the microassembly design for removing the residual mechanical stresses (RMS) is also summarized in the achievement of relatively low uncompensated error for long-term stability during 1 year for the zero signal $dU_{0\ stab}$ < 0.15 %/FS and sensitivity $dU_{0\ stab}$ < 0.20/FS.**



***Index Terms*— pressure sensor, microassembly design, high proof pressure, low error, residual mechanical stress.**

I. Introduction

THE market of microelectromechanical systems (MEMS) piezoresistive pressure sensor is experiencing steady growth due to increasing demand in automotive, aerospace, consumer applications, healthcare, nuclear energy, oil and gas industry, automated manufacturing and other areas [1]. One of the main vectors of MEMS pressure sensor development is the reduction of square chip and the change of technological route and equipment for production with larger-diameter wafer. In turn, these decisions lead to a reduction in future production costs and, as a result, an improvement in the company's competitiveness. A mandatory condition is to maintain the quality of the output characteristics of pressure sensors at the same level during production modernization. The potential use of new solutions to achieve specific application conditions, for example, by changing the design and technology of pressure sensor chip to increase manufacturing production capacity, as well as by reducing the volume of the sensor [2], changing materials for both traditional and flexible pressure sensors [3,4], the electrical circuit [5-9] and joint use with sensors of other physical quantities [10,11] requires years to confirm the patterns of maintaining or improving characteristics with dozens of repetitions upon launching a batch of wafers into production. In this case, a significant factor for development is not only the repeatability of characteristics from batch to batch, but also the stability of all parameters over time within one batch. The current focus is not only analyzing of long-term stability for useful signal, but also the change in errors for mechanical characteristics over time [12-14].

The presented study is based entirely on experimental analysis, taking into account a large statistical data set on samples, where solutions related to both the modernization of design features for the microassembly structure and the effects of changes in mechanical characteristics of differential pressure sensors on preliminary operation. The first distinctive feature of developed microassembly structures is the presence of stops on both sides of chip to achieve advantages in overload capacity by proof pressure. There are many known variants of chips and its microassembly design with stops, which were implemented by researchers from Xi'an Jiaotong University [15-19]. The development in publication [19] demonstrates the achievement of record sensitivity S = 60.0 mV/V/kPa for pressure range of 0.5 kPa with low nonlinearity $2K_{NL}$ = 0.30%/FS, mechanical hysteresis H = 0.16%/FS and repeatability R = 0.26%/FS. The microassembly comprises a step-type stop structure on a glass base, which allows to increase the proof pressure when pressure is applied from the front side of chip to 105 kPa. Disadvantage is the lack of statistical data between samples in a batch on

This work was supported by the Dukhov All-Russia Research Institute of Automatics (VNIIA). (Corresponding author: Mikhail Basov).

M. Basov is with VNIIA, Moscow 127055, Russian Federation (e-mail: engineerbasovm@gmail.com).

XXXX-XXXX © XXXX IEEE. Personal use is permitted, but republication/redistribution requires IEEE permission.
See http://www.ieee.org/publications_standards/publications/rights/index.html for more information.

variation of mechanical characteristics and the moment of membrane touching with stop. The ability to increase the proof pressure depends not only on the proposed design, but also on the pressure range. For example, pressure sensor chip with high range [20] used the process of creating a vacuum cavity for measuring absolute pressure with the formation of the cavity height to stop the membrane deflection under proof pressure. This pressure sensor design for range of up to 2.5 MPa is capable of withstanding overloads of up to 18 MPa. The presented study demonstrates the operation of a new microassembly design with mechanical stops. The microassembly design is packaged in TO-8 type Kovar package for differential pressure sensors with adjustable ranges, where the lower limit is up to 10 kPa and the upper limit is up to 60 kPa. The presence of mechanical stops on both sides of pressure sensor chip prevents the membrane damage when proof pressure of 1.5 MPa acts from either side.

The second most important distinctive feature of this study is the consideration of the issue related to improving the parametric characteristics of serially produced MEMS differential pressure sensors by reducing residual mechanical stresses (RMS) due to the optimization of microassembly design for the chip and preliminary operation by thermocycling (TC) and barocycling (BC). The advantages of reducing sensor errors in mechanical characteristics and the results of the influence of all possible design nuances and production technology will be substantiated with taking into account large experimental statistical data. The comparative relevant analysis of output parameters with other pressure sensors based on piezoresistive effect must have the approximate coincidence in the type and range of pressure, sensitivity and proof pressure indicators. Important factors such as the design and manufacturing technology of pressure sensor chip itself are very diverse and are not taken into account in the analysis. The output characteristics of development will be analyzed directly with mass-produced analogues to confirm the relevance of the proposed solutions [21].

II. Design and Technology of Pressure Sensor

A. Features of pressure sensor chip creating

The information on the design and manufacturing technology of pressure sensor chip for differential pressure range up to 10...60 kPa is presented as fixed data, since the main objective of the study is related to the specifics of practical analysis for the selected geometry of microassembly design and preliminary operations by TC and BC. The MEMS pressure sensor microassembly design utilizes pressure sensor chip with Wheatstone bridge circuit and four piezoresistors (PRs), where a membrane structure creates only on the back side of chip. A detailed description of topological and technological features of the implementation of the front side (Fig. 1a) was presented in the articles [22,23], therefore, only the main characteristics will be indicated below.

The pressure sensor chip is made by n-type monocrystalline silicon wafers with resistivity of ρ = 4.5 Ohm·cm, crystallographic plane of (100) and thickness of W_{sub} = 410 μm. The PRs on the front side of pressure sensor chip is formed by two p-type regions, united by 0.8 μm thick Al metallization on a non-deformable region of chip frame at a distance of at least 80 μm from the edge of the membrane etching wedge. A low-boron-doped region of p^--type PR with a surface concentration of $N_S = 6 \cdot 10^{18}$ cm^{-3} (surface resistance R_S = 200 Ohm/□, p-n junction depth x_j = 2.2 μm) and dimensions of 20x400 μm along the crystallographic direction [110] is the basis for the functioning of piezoresistive effect with coefficient equal to $\pi_{44} = 1.26 \cdot 10^{-9}$·Pa^{-1} at room temperature. A high-boron-doped region of the p^+-type PR with a surface concentration of $N_S = 5 \cdot 10^{19}$ cm^{-3} (surface resistance R_S = 20 Ohm/□, p-n junction depth x_j = 4.0 μm) with a relatively low piezoresistive coefficient equal to $\pi_{44} = 0.73 \cdot 10^{-9}$·Pa^{-1} is created to connect the low-boron-doped region of PR with metallization on the area of thinned part of membrane. This is necessary to eliminate the additional influence of RMS and parasitic effects from the difference of coefficients of temperature expansion (CTE) between silicon and aluminum. The high-boron-doped region of the p^+-type PR is less than 12% of the nominal resistance of the TP (R_{PR} = 5.0 ± 0.2 kOhm). Additionally, the highest potential is applied to the substrate to close the p-n junction from leakage current components that cause additional sensor errors, especially at elevated temperatures; a high-phosphorus-doped n-type region is created for ohmic contact. Silicon oxide with a thickness of W_{SiO2} from 0.18 to 0.42 μm is used as an insulation layer on the front side of chip, which thickness is depending on the doping areas by lithography. The leakage current at p-n junctions at room temperature and without exposure to external light does not exceed the values of I_{leak} < 10 nA with a reverse bias of U_{rev} = 40 V, which in part guarantees the achievement of low errors in long-term stability by the operation of the chip itself. The mobile charge in the insulation layer of Na^+, Cl^- and other element ions did not exceed $Q < 5 \cdot 10^{10}$ C/cm^2 after each oxidative diffusion process.

A membrane structure with three separate mechanical stress (MS) concentrators in the form of rigid islands (RIs) is selected (Fig. 1b) for the mechanical part of chip, where the RI thickness is equal to the initial thickness of wafer. The selected membrane structure with RIs allows for the concentration of high MS at low deflection values, which reduces the nonlinearity error. The geometry of membrane takes into account the use of liquid anisotropic etching in a 30% KOH solution at temperature of T = 85 ºC, which requires an additional area of the chip due to the etching of silicon at an angle of 54.7°. The isotropic etching of about 6 μm in a HF:HNO_3:CH_3COOH (2:9:4) solution is used to smooth out the region between the RI wedge and the thinned part of membrane at the final stage of membrane creation. It helps to increase the mechanical strength of structure the MS is actually preserved. In results, the required sensitivity for adjustable ranges up to 10...60 kPa is achieving on chip with the length of the square area A_{chip} = 4000 μm, the length of the square thinned part of membrane A_{memb} = 2200 ± 4 μm, thickness of the thinned part of membrane W_{memb} = 29 ± 2 μm,

as well as the length of RI wedge L_{RI} = 600 ± 80 μm and the gap between RI d_{RI} = 22 ± 4 μm. The geometry of mechanical part for pressure sensor chip is designed to achieve a sensitivity of at least S = 0.45 mV/V/kPa with a nonlinearity error of no more than $2K_{NL}$ = 0.20%/FS for pressure range up to 60 kPa.

B. Features of microassembly design

The main idea of this development is analysis of influence of microassembly design for pressure sensor chip, which is necessary both for the correct mechanical decoupling of the chip from the Kovar package and from the microassembly design itself, and for a critical increase in mechanical strength from either side. As mentioned earlier in the Introduction, the research presents practical statistical data, which collectively takes into account the influence of all possible design nuances and manufacturing technology of pressure sensor, since often a model of the complete microassembly design in software cannot take into account all possible nuances in multi-factorial production operations. There are many different methods known for joining the elements of a microassembly structure together, such as: hydrophilic or hydrophobic silicon bonding [24], anodic bonding [15-19, 25], eutectic bonding [26], adhesive bonding [27], reactive bonding [28], thermo-compression bonding [29], or laser bonding [30]. In this study, the bonding mechanism for the microassembly structure uses a glass frit [31, 32], since (by analogy with the implementation of pressure sensor chip based on the piezoresistive effect) the choice of this connection mechanism is justified by existing experience and previously obtained advantages in production. The use of glass frit also takes into account the fact that it has little effect on the microassembly structure chip under all-round high-pressure compression of 16 MPa, which is one of the conditions for the application of this development. If the mechanism for increasing mechanical strength by creating stops was discussed earlier, then solutions for reducing the impact of mechanical failures from microassembly structure can be judged by the identified trends from a review of similar current developments [33-46]. Among the analogies considered, articles from a group of researchers from the University College of Southeast Norway [38,41,45,46] stand out in particular, since the projects discuss many important issues regarding the RMS influence on various features of microassembly design and technology. The main trend in the general overview is to reduce the area of connection between the microassembly structure and Kovar package, as well as to use a larger volume of base by increasing the height of base as much as the space of the package allows. Additionally, it is necessary to optimally eliminate potential stress concentrators in the base if it contains sharp corners. The proposed microassembly design within Kovar pressure sensor package is schematically shown in Figure 2.

Figure 3 shows a brief technological route for the microassembly design. A monocrystalline silicon wafer with crystallographic plane of (100) and thickness of W_{base} = 3000 μm is used to create the base of the microassembly. A layer of silicon nitride Si_3N_4 by LPCVD process with thickness of W_{Si3N4} = 0.15 μm is deposited on both sides of wafer. Next, a hole with a diameter of H = 0.25 mm is formed by laser, then the structure of the lower part of base is formed as a square pedestal to a depth of G = 1.00 mm and with a curvature radius of R = 0.30 mm (Fig. 1a, b), as well as a bottom mechanical stop to a depth of B = 6 μm and with an area of A_{stop} = 1.90 x 1.90 mm^2 on the upper plane of the base.

The square pedestal side of the base for connecting the microassembly structure to the Kovar package is J = 2.70 mm. The next iterations involved cutting the wafer into bases and removing the layer Si_3N_4, which was needed as a barrier against the fusion of silicon dust splashes during laser processing. At the final stage, isotropic etching of all sides of the base structure occurs at 50 μm to reduce the influence of MS concentrators. The top mechanical stop of microassembly structure is created from monocrystalline silicon wafer with crystallographic plane of (100) and thickness of F = 380 μm by cutting into elements with an area A_{cover} = 2.60 x 4.00 mm^2. A layer of glass frit is applied on a robotic unit to the upper surface of base along the perimeter and to one of the surfaces of top mechanical stop along the two smaller sides of the area. The layer of glass frit is vitrified at T_{vit} = 520 °C for t_{vit} = 1 hour. The final connection of all elements into the microassembly structure occurs by soldering in a vacuum P_{vac} = $3 \cdot 10^{-4}$ Pa at a temperature T_{sold} = 397 °C for t_{sold} = 20 minutes and a torque M = 0.7 N*m (the torque acts only during the middle 10 minutes of the process). The top mechanical stop is centered relative to the pressure sensor chip during soldering to keep the contact pads open for further ultrasonic welding. The spaces between the pressure sensor chip and the long sides of the top mechanical stop are open to allow pressure to be applied from the front side of chip. The resulting gaps E = 23 ± 2 μm and C = 29 ± 3 μm (Fig. 2a) in this soldering mode between the elements of the microassembly structure differ by an amount equal to the height of bottom mechanical stop B = 6 μm, since the volume of glass frit applied to the base is greater than glass frit layer on the top mechanical stop. As can be seen from Fig. 4a, excess frit volume during vacuum soldering of elements can extend beyond the area of the connection between the chip and base. Insufficient glass frit volume at the joint is undesirable, as it can increase the likelihood of microcracks or voids. The resulting gap dimensions are necessary for the free movement of pressure sensor chip membrane when nominal pressure up to 60 kPa is applied from either side, as well as for timely contact with the upper or bottom mechanical stop before destruction from proof pressure.

The connection of microassembly structure with Kovar package is achieved by organosilicon glue. The process of applying and drying the organosilicon adhesive also has a significant effect on the RMS for pressure sensor chip [40,42], therefore, it is necessary to hold the assembly for 24 hours under normal climatic conditions and then only use drying at T_{dry} = 250 °C for t_{dry} = 1 hour after uniformly applying the adhesive to the lower surface of base. The condition of tightness of all connections inside the pressure sensors from helium leakage with indicators of no worse than $1 \cdot 10^{-9}$ $m^3 \cdot Pa \cdot s^{-1}$

is met (Fig. 4b, c) to ensure that pressure is supplied only from the front side of pressure sensor chip through the hole in package cover or from the back side of pressure sensor chip through the tube of package base. Electrical insulation of Kovar package from the pressure sensor chip is no worse than 1 GΩ at 100 V.

More than 120 samples of developed pressure sensor are analyzed to conduct further statistical studies on the effects of proof pressure and mechanical characteristics.

III. Experimental studies

A. The influence of proof pressure

There are a number of features during the production of developed pressure sensor that affect the indicators of technological waste from batch to batch and from sample to sample. It is necessary to guarantee the precision of chip membrane touching with stops during the vacuum soldering process. In turn, the chip membrane touching with the stops depends on:

1. The membrane thickness, which determines its deflection when pressure is applied. There is a technological variation in the chip membrane thickness both within the area of a 4-inch diameter wafer and between wafers, which can reach up to 10-15% of its nominal value between samples.
2. Repeatability of the vacuum soldering process by temperature. Process temperature significantly depends on the choice of thermocouple for actual value analysis, pressure for vacuum, heating mechanism and many other equipment features.
3. The spread of the height of the bottom stop at the base, which is currently about ±2 μm.
4. Uniform glass frit application to the base and top mechanical stop. The glass frit application thickness depends not only on the application mode but also on the glass frit's density and grain size across all grinding fractions, which may vary from process to process.

Due to the presence of process waste, the membrane may be touched on the top and bottom stops either prematurely, which leads to a high nonlinearity error, or late touching, which leads to membrane destruction when overloaded with a proof pressure of less than 1.5 MPa. Currently, the combination of all factors allows us to obtain approximately 88% of developed pressure sensor samples that have the correct moments of membrane touching with stops.

The graphs show that the moments of membrane touching with the top stop occurs in a narrower pressure range of 200 to 600 kPa, in contrast to the touching with base in the range of 200 to 800 kPa, which is likely due to both the greater unevenness of the glass frit application on the base surface and the continued deflection of membrane after touching only by the middle RI. Tests on the impact of proof pressure were carried out inside the thermal chamber Espec MC-811, which provides temperature fluctuation at a point up to ΔT_{thermo} = ±0.5 ºC and temperature gradient across the chamber volume up to $\Delta T'_{thermo}$ = ±2.0 ºC in the range from -65 ºC to +85 ºC. The temperature parameters of chamber are significantly lower even the useful volume is filled with samples in the fixture to more than 50% as it is proved by thermal chamber certification. The temperature inside the chamber is constantly maintained at +30°C without the use of a refrigerator during proof pressure analysis to eliminate noise of output signal from vibration. The pressure by air is set using WIKA Mensor CPC8000 with module up to 5 MPa and its accuracy class of 0.01%. National Instruments PXI-1044 system with PXI-4132 power supply (task maintenance accuracy up to 0.025% over a year), PXI-4071 multimeter unit (measurement accuracy up to 0.001% over 90 days) and PXI-2527 multiplexer are used to voltage supply (U_{supply} = 5 V) and measurement the output signal. This set of equipment is subsequently used in the analysis of all mechanical characteristics. The measurement of error by changing of zero signal and sensitivity after proof pressure of P_{proof} = 1.5 MPa is carried out under the condition of exposure to the proof pressure itself for 5 minutes and a holding time of 10 minutes after removal of proof pressure. All parameter and error indicators are presented as “arithmetic mean ± standard deviation” in Table 1 and further, where critical excesses in indicators are present, amount to less than 4% for all types of parameters and are not taken into account in the statistical data. The lowest nominal pressure of 10 kPa is considered to calculate the errors in the effect of proof pressure, since the indicators of this parameter have the highest values relative to the parameters for other pressure ranges up to 60 kPa. All parameters in Table 1 are the main uncompensated error, as, for example, temperature hysteresis and long-term stability. These parameters are significantly reduced by increasing the time after exposure to proof pressure to allow for greater mechanical relaxation of microassembly structure.

B. 3.2. The mechanical characteristics before and after TC and BC

All mechanical parameters for zero signal, sensitivity, nonlinearity, mechanical hysteresis and mechanical repeatability are analyzed by placing the pressure sensors inside the thermal chamber at temperature of +30 ºC without using a refrigerator as in the case of proof pressure analysis. The study of all mechanical parameters is carried out both with pressure applied from the back side and front side of chip. The calculation of error based on mechanical characteristics is carried out for the widest pressure range up to 60 kPa, which guarantees lower error values for intermediate ranges below up to 10 kPa. The pressure setting is also carried out using WIKA Mensor CPC6050 with module for 100 kPa and its accuracy class of 0.01%. Measurements of output signal occur after 1 minute of holding time after setting the required pressure. Tests of all mechanical characteristics were carried out before and after TC and BC. The selection of modes and methods for TC and BC is based on the AEC-Q100 and AEC-Q103 specifications by Automotive Electronics Council (AEC) [47]. The TC is performed in temperature range from -65°C to +130°C and consists of 50 temperature cycles over 150 hours. 40,000 BC are also performed at elevated temperature of +110°C under a pressure of 100 kPa

applied from the back of chip. Table 2 presents the mechanical characteristics before and after TC and BC.

If we evaluate the indicators from the statistic of samples, so we can note a significant reduction of RMS influence of assembly design on pressure sensor chip:

1. The average zero signal values are reduced by approximately 7% and the spread between samples is also reduced after TC and BC.
2. The output signal (sensitivity) changes when pressure is applied to the back and front sides of chip differed before TC and BC tests. This difference is reduced by 2x times from 0.4 mV/5V/60kPa to 0.2 mV/5V/60kPa after TC and BC tests, and currently amounts to approximately 1% of the average values. It is likely that the remaining RMS slightly compress the thinned part of membrane, since sensitivity is higher when pressure is applied to the front side and it can bend toward the top mechanical stop.
3. The average sensitivity values of S = 0.61 ± 0.15 mV/V/kPa increased by approximately 3%.
4. The nonlinearity values for pressure applied to the back and front sides of chip also differed before TC and BC tests. The difference in values decreased from 0.038%/FS to 0.029%/FS after TC and BC tests. It indicates that the entire microassembly structure is approaching equilibrium. The remaining error difference is likely a consequence of the mechanical structure of chip membrane itself. The significant reduction in the spread of nonlinearity errors between samples relative to the mean value by approximately 22%.
5. TC and BC have a significant impact on the mechanical hysteresis H and mechanical repeatability R values. The average mechanical hysteresis H values decreased by 3.2X and 5.5X times for pressure applied from the back and front sides of chip, respectively. The average mechanical repeatability R values decreased by 1.9X and 4.0X times for pressure applied from the back and front sides of chip, respectively. The sample variations spread in these parameters also decreased.

Additionally, the samples are tested for the effect of all-round compression by pressure of 16 MPa, which is another important parameter declared by the operating conditions of this development at the consumer. The error of changing of zero signal on all-round compression are dU_{comp} = 0.089 ± 0.056%/FS for pressure range up to 60 kPa. Some number of samples is analyzed for changing of zero signal and sensitivity over 1 year for the lowest pressure range up to 10 kPa, which ensures lower error rates for intermediate ranges up to 60 kPa. The long-term stability parameters are measured while maintaining a number of conditions regarding the temperature inside the chamber at +30 ºC, the number and locations of samples inside the chamber and the use of all measuring instruments and equipment for testing. The samples were disconnected from the power supply and stored outside the thermal chamber between measurements on different days. The long-term stability error of zero signal is $dU_{0\ stab}$ = 0.097 ± 0.045%/FS, while the long-term stability of sensitivity is slightly higher $dU_{P\ stab}$ = 0.141 ± 0.056%/FS. One of the reasons for the increase error by long-term stability of sensitivity could be the instability of maintaining the temperature at a point inside the thermal chamber over the course of 1 year. This has a significant impact on sensitivity, since the temperature coefficient of sensitivity is actually an order of magnitude higher relative to the temperature coefficient of zero signal and, for example, it can lead to an additional component of error by long-term stability of sensitivity of $\Delta dU_{0\ stab}$ = 0.026%/FS when the temperature changes by 0.1 ºC over the course of 1 year.

IV. Experimental studies

Table 3 presents the output characteristics of pressure sensors produced by various companies [21] with an analog non-amplified output signal, the types of which are closest to each other in terms of differential pressure range, sensitivity and proof pressure. The developed pressure sensor and its analogues certainly have its own advantages and disadvantages, which in turn determine the specific nuances of applicability in various industrial areas. The pressure sensor PT2710 by Amphenol NovaSensors and TSC016KD by Honeywell are worth noting. The PT2710 pressure sensor is designed for range up to 17 kPa (2.5 psi), which is close to the lower range limit of developed pressure sensor. However, the analog's sensitivity is 2.3X times higher while chip surface area 5X times smaller. Another advantage of microassembly design for the PT2710 pressure sensor is its record-low error for long-term stability. The advantages of the developed pressure sensor compared to the PT2710 are the possibility of proof pressure increasing by almost 9X times, and also it is possible to maintain low nonlinearity errors (in a range 3.5 times greater than the range of the analog). If we consider the TSC016KD analogue by Honeywell for pressure range up to 16 kPa, so its sensitivity is 2X times lower than sensitivity of the developed pressure sensor, but at the same time, the set of all mechanical characteristics has lower errors, but not significantly. The advantages of the developed pressure sensor compared to the TSC016KD pressure sensor include the ability to increase the impact of proof pressure by almost 7.5X times and the lower limit of the burst pressure by 5.0X times. The general distinguishing feature of the developed pressure sensor from its mass-produced analogues is the annual production volume, which is several orders of magnitude higher than the production of the developed sensors.

V. Conclusion

The presented development of piezoresistive MEMS pressure sensor for differential pressure adjustable ranges up to 10…60 kPa with a sensitivity of S = 0.61 ± 0.15 mV/V/kPa has significant advantages over analogs in terms of multiple increase of proof pressure P_{proof} up to 1.5 MPa from either side of chip, where the condition for detecting the limit value is not exceeding the error in changing the zero signal and sensitivity up to 0.3%/FS. The project achieved low performance across all error types due to the new microassembly design for pressure sensor, despite the presence of additional element in the form of top mechanical stop and glass frit connection areas

on the front side of chip, which are the cause of increased RMS. The parameters of the developed pressure sensor are calculated for adjustable differential pressure ranges with the lower limit up to 10 kPa, which is used to analyze errors in long-term stability; and the upper limit of up to 60 kPa, which is used to analyze errors in nonlinearity, the impact of proof pressure on either side of chip, mechanical hysteresis and mechanical repeatability, as well as the impact of all-round compression. All mechanical characteristics of the developed pressure sensor is analyzed with pressure applied both from the back and front side of chip. This research also demonstrated the advantages in reducing errors with varying degrees of effectiveness after conducting additional TC and BC with the aim of reducing RMS by different mechanical connections of pressure sensor chip with package.

It is possible to achieve low error values for nonlinearity ($2K_{NL}$ < 0.20%/FS), mechanical hysteresis (H < 0.10%/FS), and mechanical repeatability (R < 0.05%/FS), as well as for the effect of all-round compression at a pressure of 16 MPa (dU_{comp} < 0.15%/FS) after TC and BC tests on over 120 samples of developed pressure sensor. The significant advantage of this design is also summarized by the achievement of relatively low basic uncompensated errors of long-term stability for 1 year for the zero signal $dU_{0\ stab}$ < 0.15 %/FS and sensitivity $dU_{P\ stab}$ < 0.20 FS.

REFERENCES

[1] Pressure Sensor Chip Market Size, Competitive Assessment & Forecast. Available online: https://www.verifiedmarketreports.com/product/pressure-sensor-chip-market/

[2] Huang, M., Wu, X., Zhao, L., Han, X., Xia, Y., Gao, Y., Cui, Z., Zhang, C., Yang, X., Qiao, Z., Li, Z., Han, F., Yang, P., Jiang, Z. Small-size temperature/high-pressure integrated sensor via flip-chip method. Microsyst Nanoeng 2024, 10, 104

[3] Schauss, G., Hayman, A.P.A. A Taxonomy of Pressure Sensors for Compression Garment Development. Sensors. 2025, 25, 4445.

[4] Tao, L.-Q., Zhang, K.-N., Tian, H., Liu, Y., Wang, D.-Y., Chen, Y.-Q., Yang, Y., Ren, T.-L. Graphene-Paper Pressure Sensor for Detecting Human Motions. ACS Nano, 2017, 11, 8790–8795.

[5] Basov, M. High-Sensitivity MEMS Pressure Sensor Utilizing Bipolar Junction Transistor with Temperature Compensation. Sens Actuators A Phys 2020, 303, 111705.

[6] Basov, M. Ultra-High Sensitivity MEMS Pressure Sensor Utilizing Bipolar Junction Transistor for Pressures Ranging From −1 to 1 KPa. IEEE Sens J 2021, 21, 4357–4364.

[7] Basov, M. Development of High-Sensitivity Pressure Sensor with on-Chip Differential Transistor Amplifier. Journal of Micromechanics and Microengineering 2020, 30, 065001.

[8] Basov, M. High Sensitive, Linear and Thermostable Pressure Sensor Utilizing Bipolar Junction Transistor for 5 KPa. Phys Scr 2021, 96, 065705.

[9] Basov, M. Pressure Sensor with Novel Electrical Circuit Utilizing Bipolar Junction Transistor. In Proceedings of the 2021 IEEE Sensors; IEEE, October 31 2021; pp. 1–4.

[10] Han, X., Huang, M., Wu, Z., Gao, Y., Xia, Y., Yang, P., Fan, S., Lu, X., Yang, X., Liang, L., Su, W., Wang, L., Cui, Z., Zhao, Y., Li, Z., Zhao, L., Jiang, Z. Advances in high-performance MEMS pressure sensors: design, fabrication, and packaging. Microsyst Nanoeng, 2023, 9, 156

[11] Basov, M. Schottky Diode Temperature Sensor for Pressure Sensor. Sens Actuators A Phys 2021, 331.

[12] Liu, S.; Du, X.H.; Zhu, M.J.; Liu, D. Long-Term Stability Enabling Technology of Silicon-Based Piezoresistive MEMS Pressure Sensor. J Phys Conf Ser 2020, 1520, 012009.

[13] Basov, M. Research of MEMS Pressure Sensor Stability With PDA-NFL Circuit. IEEE Sens J 2024, 24, 34083-34090.

[14] Basov, M. Research of Long-Term Stability of High-Sensitivity Piezoresistive Pressure Sensors for Ultralow Differential Pressures. IEEE Sens J 2024, 24, 36443-36450.

[15] Yu, Z.; Zhao, Y.; Li, L.; Li, C.; Liu, Y.; Tian, B. Realization of a Micro Pressure Sensor with High Sensitivity and Overload by Introducing Beams and Islands. Microsystem Technologies 2015, 21, 739–747.

[16] Z. Yu, Y. Zhao, L. Sun, B. Tian, Z. Jiang. Incorporation of beams into bossed diaphragm for a high sensitivity and overload micro pressure sensor, Rev. Sci. Instrum., 2013, 84, 015004.

[17] Meng, X.; Zhao, Y. The Design and Optimization of a Highly Sensitive and Overload-Resistant Piezoresistive Pressure Sensor. Sensors 2016, 16, 348.

[18] Yu, Z., Zhao, Y., Li, C., Liu, Y., Zhou, G., Tian, B.A micro-pressure sensor with high sensitivity and overload resistance. In Proceedings of the 2013 IEEE Sensors; IEEE, 2013, Baltimore, MD, USA, pp. 1-4.

[19] Xu, T.; Lu, D.; Zhao, L.; Jiang, Z.; Wang, H.; Guo, X.; Li, Z.; Zhou, X.; Zhao, Y. Application and Optimization of Stiffness Abruption Structures for Pressure Sensors with High Sensitivity and Anti-Overload Ability. Sensors 2017, 17, 1965.

[20] C. Rongyan, W. Jian, Y. Chang, D. Quan, Y. Lijian. High Overload Pressure Sensor Construct with Polysilicon Nanofilm. IEEE Sensors Journal, 2015, 15, 1414-1420.

[21] Digikey. Available online: https://www.digikey.com/

[22] Basov, M.; Prigodskiy, D.M. Investigation of High-Sensitivity Piezoresistive Pressure Sensors at Ultra-Low Differential Pressures. IEEE Sens J 2020, 20, 7646–7652.

[23] Basov, M.; Prigodskiy, D. Development of High-Sensitivity Piezoresistive Pressure Sensors for −0.5…+0.5 KPa. Journal of Micromechanics and Microengineering 2020, 30, 105006.

[24] Handbook of Wafer Bonding; Ramm, P., Lu, J.J., Taklo, M.M. V., Eds.; Wiley, 2012; ISBN 9783527326464.

[25] Kober, T.; Werthschützky, R. Wafer Level Processing of Overload-Resistant Pressure Sensors. Procedia Eng 2012, 47, 615–618.

[26] Liu, Q.; Du, L.; Zhao, Z.; Xiao, L.; Sun, X. Localized Si–Au Eutectic Bonding around Sunken Pad for Fabrication of a Capacitive Absolute Pressure Sensor. Sens Actuators A Phys 2013, 201, 241–245.

[27] Wandowski, T.; Moll, J.; Malinowski, P.; Opoka, S.; Ostachowicz, W. Assessment of Piezoelectric Sensor Adhesive Bonding. J Phys Conf Ser 2015, 628, 012114.

[28] Schumacher, A.; Shah, V.; Steckemetz, S.; Dietrich, G.; Pflug, E.; Hehn, T.; Knappmann, S.; Dehé, A.; Leson, A. Improved Mounting of Strain Sensors by Reactive Bonding. J Mater Eng Perform 2021, 30, 7796–7804.

[29] Wang, Q.; Yang, X.; Zhang, Y.; Ding, J. A Simple Thermo-Compression Bonding Setup for Wire Bonding Interconnection in Pressure Sensor Silicon Chip Packaging. Microsystem Technologies 2011, 17, 1629–1633.

[30] Kim, S.; Park, J.; So, S.; Ahn, S.; Choi, J.; Koo, C.; Joung, Y.-H. Characteristics of an Implantable Blood Pressure Sensor Packaged by Ultrafast Laser Microwelding. Sensors 2019, 19, 1801.

[31] Chang, J.-S.; Lin, J.-Y.; Ho, S.-C.; Lee, Y.-J. Wafer Level Glass Frit Bonding for MEMS Hermetic Packaging. In Proceedings of the 2010 5th International Microsystems Packaging Assembly and Circuits Technology Conference; IEEE, October 2010; pp. 1–4.

[32] Knechtel, R.; Zellmer, M.; Schikowski, M.; Behmueller, M.; Van Buggenhout, C.; Petropoulos, A. Glass Frit Wafer Bonding for Encapsulating Monolithic Integrated CMOS-MEMS Devices. ECS Trans 2018, 86, 111–118.

[33] Li, L.; Belov, N.; Klitzke, M.; Park, J.-S. High Performance Piezoresistive Low Pressure Sensors. In Proceedings of the 2016 IEEE SENSORS; IEEE, 2016; pp. 1–3.

[34] Waber, T., Pahl, W., Schmidt, M., Feiertag, G., Stufler, S., Dudek, R., Leidl, A. Temperature characterization of flip-chip packaged piezoresistive barometric pressure sensors. Microsyst Technol, 2014, 20, 861–867.

[35] Krondorfer, R.H., Kim, Y. K. Packaging Effect on MEMS Pressure Sensor Performance. IEEE Transactions on Components and Packaging Technologies, 2007, 30, 285-293

[36] Hamid, Y.; Hutt, D.A.; Whalley, D.C.; Craddock, R. Relative Contributions of Packaging Elements to the Thermal Hysteresis of a MEMS Pressure Sensor. Sensors 2020, 20, 1727.

[37] Lishchynska, M., O'Mahony, C., Slattery, O., Wittler, O., Walter, H. Evaluation of Packaging Effect on MEMS Performance: Simulation and Experimental Study. IEEE Transactions on Advanced Packaging, 2007, 30, 629-635

[38] Sandvand, Å., Halvorsen, E., Aasmundtveit, K.E., Jakobsen, H. Influence of Glass-Frit Material Distribution on the Performance of Precision Piezoresistive MEMS Pressure Sensors. IEEE Transactions on Components, Packaging and Manufacturing Technology, 2015, 5, 1559-1566.

[39] Walwadkar, S.S., Cho, J. Evaluation of die stress in MEMS packaging: Experimental and theoretical approaches. IEEE Trans. Compon. Packag. Technol., 2006, 29, 735–742

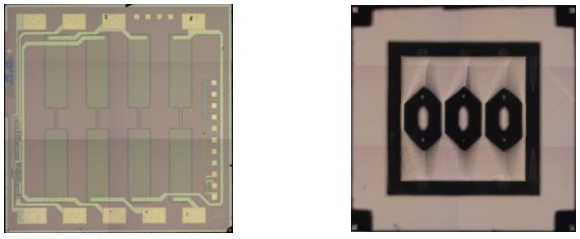
[40] Albert Chiou, J., Chen, S. Pressure nonlinearity of micromachined piezoresistive pressure sensors with thin diaphragms under high residual stresses. Sensors and Actuators A: Physical, 2008, 147, 332–339.

[41] Sandvand, A.; Halvorsen, E.; Aasmundtveit, K.E.; Jakobsen, H. Identification and Elimination of Hygro-Thermo- Mechanical Stress-Effects in a High-Precision MEMS Pressure Sensor. J.l of Microel. Syst. 2017, 26, 415–423.

[42] Zarnik, M.S.; Rocak, D.; Macek, S. Residual Stresses in a Pressure-Sensor Package Induced by Adhesive Material during Curing: A Case Study. Sens Actuators A Phys 2004, 116, 442–449.
[43] Tamaki I.; Tetsu O.; Masaaki N.; Etsutaro K.; Tetsurou T.; Ryuuzou A. New DPharp Series Pressure and Differential Pressure Transmitters. Yokogawa Technical Report English Edition 2004, 9–14.
[44] Wang, J.; Li, X. Package-Friendly Piezoresistive Pressure Sensors with on-Chip Integrated Packaging-Stress-Suppressed Suspension (PS 3) Technology. Journal of Micromechanics and Microengineering 2013, 23, 045027.
[45] Sandvand A. High-stability piezoresistive pressure sensors: PhD dissertation in Applied Micro- and Nanosystems. Kongsberg – 2017
[46] Sandvand, Å., Halvorsen, E., Jakobsen, H. In Situ Observation of Metal Properties in a Piezoresistive Pressure Sensor. Journal of Microelectromechanical Systems, 2017, 26, 1381-1388.
[47] Automotive Electronics Council (AEC). Available online: https://www.aecouncil.com.



Mikhail Basov graduated from the National Nuclear Research University “Moscow Engineering Physics Institute” (MEPhi, Nano- and Microelectronics department, Moscow, Russia) as MSc in Electrical and Electronics Engineering. Since 2010 he currently works as R&D Engineer focused on developing MEMS piezoresistive pressure and microelectronic temperature sensors in Dukhov Authomatic Research Institute (FSUE VNIIA, Moscow, Russia). He received the Ph.D. degree from MEPhI in 2022. His PhD thesis is about creation of new pressure sensor chip with novel piezosensitive electrical circuit utilizing bipolar-junction transistor differential amplifier with negative feedback loop (PDA-NFL). He is the author of 13 articles, 22 Russian patents, and 18 conference papers. He received the award of University Technology Exposure Program by Wevolver, Mouser Electronics and ANSYS in 2022, Innovative Leader Award in the Nuclear Industry by Rosatom in 2019, and Brish Young Scientists Competition by FSUE VNIIA in 2023.



(a) (b)

Fig. 1. Photo of pressure sensor chip: a) the front side, b) the back side.

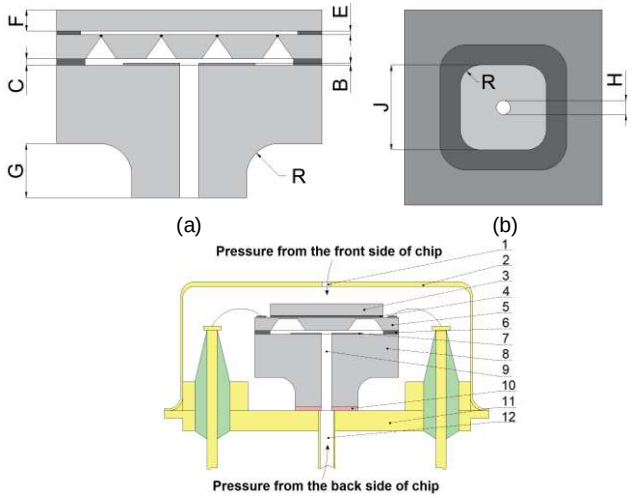


Fig. 2. Schematic representation of: a) the microassembly structure (side view), b) the microassembly structure (bottom view), c) the pressure sensor (with a side view of the microassembly structure rotated 90° relative to Fig. 1a): 1 - hole in the package cover for applying pressure from the front side of pressure sensor chip, 2 - package cover, 3 - top mechanical stop of the microassembly structure, 4 – glass frit layer for connecting the top mechanical stop and the pressure sensor chip, 5 - pressure sensor chip, 6 - glass frit layer for connecting the pressure sensor chip and the base of the microassembly structure, 7 - bottom mechanical stop formed on the upper plane of base, 8 - base of microassembly structure, 9 - hole in the base of microassembly structure, 10 - layer of organosilicon adhesive for connecting the microassembly structure and the Kovar package, 11 - base of package, 12 - tube in the base of package for applying pressure from the back sides of pressure sensor chip.

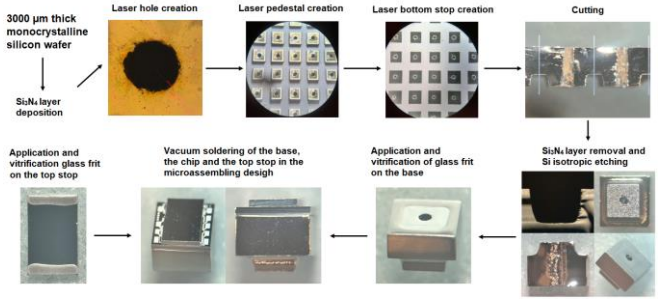
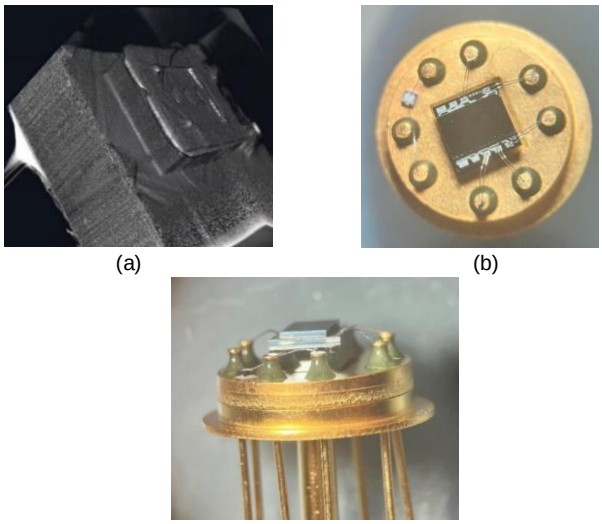


Fig. 3. Brief technological route of the microassembly design for pressure sensor.



(a) (b)

(c)

Fig. 4. Differential pressure sensor: a) tomography, b) top view without cover, c) side view without cover.

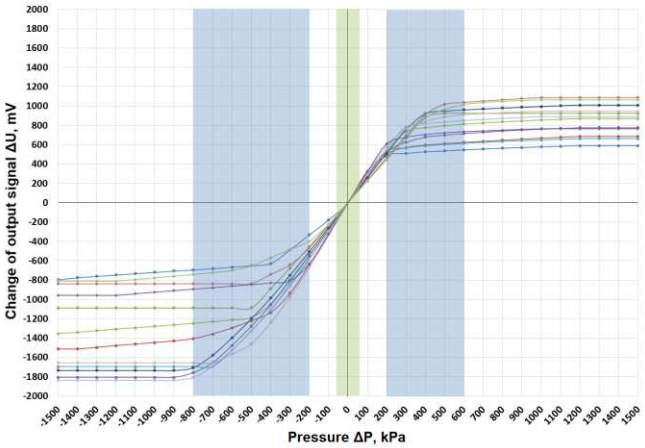


Fig. 5. The dependence of output signal for developed pressure sensors on applied pressure up to 1.5 MPa (green zone – range of nominal pressure; blue zone – range of the moment of membrane touching with stops).

TABLE I
ERROR OF CHANGES IN THE OUTPUT SIGNAL OF DEVELOPED PRESSURE SENSOR UNDER THE INFLUENCE OF A PROOF PRESSURE OF 1.5 MPA.

Parameter / Proof pressure supply side	The back side of chip	The back side of chip
Changing of zero signal $dU_{0\,Pproof}$, %/FS	0,110 ± 0,094	0,144 ± 0,136
Changing of sensitivity $dU_{P\,Pproof}$, %/FS	0,140 ± 0,053	0,181 ± 0,079

TABLE II
PARAMETERS FOR MECHANICAL CHARACTERISTICS OF DEVELOPED PRESSURE SENSOR FOR DIFFERENTIAL PRESSURE RANGE UP TO 10…60 KPA.

Parameter / Pressure supply side	Before TC and BC		After TC and BC	
	The back side of chip	The back side of chip	The back side of chip	The back side of chip
Zero signal U_0, mV	4,29 ± 6,09		4,00 ± 5,99	
Changing of output signal ΔU_P, mV	181,9 ± 45,5	182,3 ± 45,7	182,6 ± 45,7	182,8 ± 45,8
Nonlinearity $2K_{NL}$, %/FS	0,100 ± 0,093	0,062 ± 0,056	0,096 ± 0,073	0,067 ± 0,043
Mechanical hysteresis H, %/FS	0,137 ± 0,026	0,153 ± 0,029	0,042 ± 0,022	0,028 ± 0,017
Mechanical repeatability R, %/FS	0,045 ± 0,028	0,036 ± 0,036	0,024 ± 0,020	0,009 ± 0,008

TABLE III
COMPARISON OF OUTPUT MECHANICAL CHARACTERISTICS OF DEVELOPMENT WITH RESPECT TO COMMERCIALLY AVAILABLE DIFFERENTIAL PRESSURE SENSORS FROM VARIOUS COMPANIES.

Manufacturer			FSUE VNIIA	Amphenol NovaSensors	NXP	Honeywell	Acuity	TE Connectivity
Modification			-	PT2710	MPX2300DT1	TSC016KD	AC3012-005-G	SMI SM9520
Pressure range ΔP		kPa	10…60	17	40	16	35	10
Overall dimensions of microassembly		mm	4,0x4,0x3,8	2,0x1,6x1,0	-	-	1,8x1,6x0,4	2,1x2,1x0,6
Proof pressure ΔP_{proof}		MPa	1,50 (x25…150)	0,17 (x10)	0,86 (x22)	0,20 (x13)	0,17 (x5)	0,08 (x8)
Changing of zero signal and sensitivity on proof pressure dU_{proof}		%/FS	< 0,30	-	-	-	-	-
Burst pressure ΔP_{burst}		MPa	> 2,00 (x33…200)	- -	- -	> 0,40 (x25)	> 0,52 (x15)	> 0,10 (x10)
Sensitivity S		mV/V/kPa	0,61 ± 0,15	1,40 ± 0,35	0,04 ± 0,01	0,29 ± 0,02	0,63 ± 0,11	1,90 ± 0,60
Zero signal U_0		mV/V	< 2,0	< 10,0	< 0,1	< 0,1	< 10,0	< 15,0
Nonlinearity $2K_{NL}$		%/FS	< 0,20 (60 kPa)	< 0,25	< 1,50	< 0,15	< 0,10	< 0,35
Mechanical hysteresis H		%/FS	< 0,10 (60 kPa)	< 0,20			-	-
Long-term stability dU_{stab}	Zero signal	%/FS	< 0,15 (1 year)	< 0,10 (1 year)	-	< 0,10 (1000 h)	-	< 2,00 (10 years)
	Sensitivity	%/FS	< 0,20 (1 year)					-
Package			TO-8	-*	98ASB13355C	DIP/SMT/SIP	-*	-*
Presence of a temperature sensor			+	+	+	+	-	-
The presence of a compensation circuit in the housing			-	-	+	-	-	-

* - unpackaged element